

*The Nature and Evolution of Disks Around Hot Stars*  
*ASP Conference Series, Vol. TBD, 2005*  
*R. Ignace & K. Gayley*

## Diagnostics of Disks Around Hot Stars

David H. Cohen

*Department of Physics & Astronomy, Swarthmore College, Swarthmore,  
 PA 19081, USA*

Margaret M. Hanson

*Physics Department, University of Cincinnati, Cincinnati, OH 45221,  
 USA*

Richard H. D. Townsend

*Bartol Research Institute, University of Delaware, Newark, DE 19716,  
 USA*

Karen S. Bjorkman

*Department of Physics & Astronomy, University of Toledo, Toledo, OH  
 43606, USA*

Marc Gagné

*Department of Geology & Astronomy, West Chester University, West  
 Chester, PA 19383, USA*

**Abstract.** We discuss three different observational diagnostics related to disks around hot stars: absorption line determinations of rotational velocities of Be stars; polarization diagnostics of circumstellar disks; and X-ray line diagnostics of one specific magnetized hot star,  $\theta^1$  Ori C. Some common themes that emerge from these studies include (a) the benefits of having a specific physical model as a framework for interpreting diagnostic data; (b) the importance of combining several different types of observational diagnostics of the same objects; and (c) that while there is often the need to reinterpret traditional diagnostics in light of new theoretical advances, there are many new and powerful diagnostics that are, or will soon be, available for the study of disks around hot stars.

## 1. Introduction

Disks are a spatial and dynamic phenomenon, which would, ideally, be studied by direct imaging and *in situ* measurements to learn about their spatial extent and physical properties (temperature, density, ionization structure, scale height, velocity fields). Needless to say, direct imaging and *in situ* measurements will not be practical any time in the near future, although indirect imaging, via interferometry, has begun to be a reality. Thus, we must use the traditional tools of stellar astrophysics: photometry, spectroscopy, and polarimetry in order to learn about the important physical properties of the disks around hot stars.

While employing these diagnostics, it is important to bear in mind several points, most if not all of which flow from our emphasis on deriving information about the specific *physical* properties of these disks:

- It is important to not put the cart before the horse and make observations simply because new instruments become available. One must first determine what information is needed, preferably to test competing hypotheses, and then find the right diagnostic or set of diagnostics that can address the specific question.
- Interpreting the results of diagnostics is more straightforward when there is an underlying physical model, but it is also important to keep in mind that the physical model might be wrong or at least too simplistic. Theorists are most useful when their theories can make clear, quantitative predictions that can be tested by observations.
- It is important to look at the sensitivity of diagnostics to relevant parameters and to critically evaluate how much diagnostic discrimination is possible from a given observation.

There are important new diagnostics coming on line in the next few years, and our community should plan on exploiting them effectively. These include sensitive polarization measurements of Zeeman splitting and new interferometers, among others. But we should also bear in mind that some older and more traditional diagnostics can still be used profitably, and that the interpretation of old measurements can also change with new insights from theorists.

In the rest of this paper, we report on three different pieces of work involving diagnostics of hot star disks. In §2, Richard Townsend evaluates the methods for inferring stellar rotational velocities from observed line profiles. In §3, Karen Bjorkman discusses spectropolarimetric diagnostics of hot star disks. In §4, Marc Gagne combines X-ray spectroscopy with several other diagnostics to infer the physical properties of, and causal mechanisms at work in, the young magnetized O star,  $\theta^1$  Ori C. We offer some concluding remarks in §5.

## 2. Absorption Line Diagnostics: Stellar Rotational Velocities

Though not directly a diagnostic of hot star disks, photospheric absorption line diagnostics of rapidly rotating hot stars have a direct bearing on the formation mechanisms of Be disks. If these stars are typically more than  $100 \text{ km s}^{-1}$  shy of their critical velocities,  $v_{\text{crit}}$ , as is commonly assumed, then the mechanism(s) required to launch material off of their surfaces and into orbit have much more extreme energy and angular momentum requirements compared to the situation if these stars are actually rotating much closer to critical. This subject is an example of how theory and modeling can be crucial in interpreting diagnostics, even relatively old and well-established ones.

The general procedure for inferring stellar rotational velocities is to obtain stellar absorption line profiles, measure the Doppler broadening, infer the projected equatorial rotational velocity  $v_e \sin i$ , and then apply statistical analysis to derive the distribution of  $v_e$ . Surveys suggest Be stars have values of  $v_e \approx 0.7$

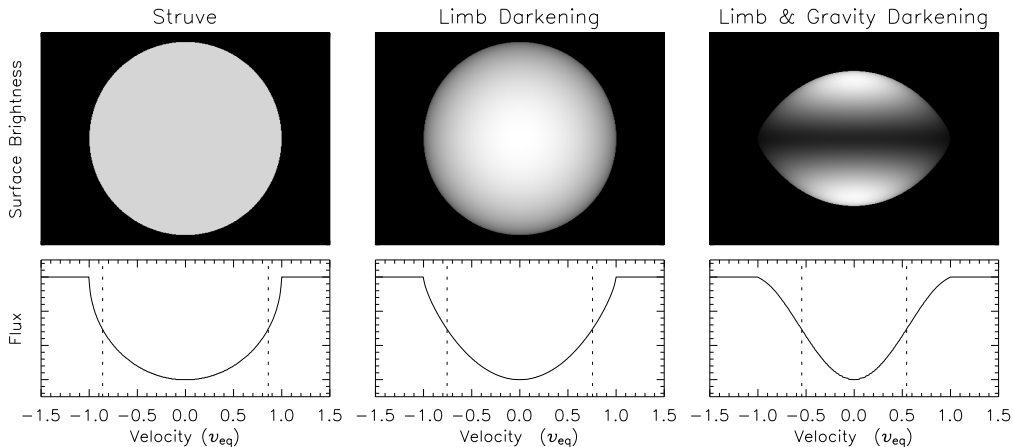


Figure 1. Schematic images three stars: uniform disk (left), limb darkened circular disk (center), oblate, gravity-darkened, and limb-darkened disk (right). The brightness is proportional to the emergent flux. The lower panels are the corresponding absorption line profile for each of the three emission models. The separation of the vertical lines indicate the full-width at half maximum (FWHM) of each profile.

to  $0.8 v_{crit}$ . However, this procedure requires a *model* of the broadening process. The original method goes back to Shajn & Struve (1929), who assumed the intrinsic emission profile from each surface patch is a delta function and ignored limb darkening (we will refer to this as the “Struve model”). In this case, isoveLOCITY contours are bands on the star parallel to the rotation axis, and the line profile mirrors the shape of the star, as in the left-hand panels of Fig. 1.

Observationally, the width of a given line can be parameterized using a measure like the FWHM or the Fourier width. In Struve’s model, these measures of the width are directly proportional to  $v_e \sin i$ , and thus measurements can be easily and unambiguously inverted to obtain a value for  $v_e \sin i$ .

We can go beyond Struve’s model and include limb darkening, which reduces the contribution from the edges of the stellar disk and thus results in a narrower, V-shaped profile than in Struve’s model, as we show schematically in the middle panels of Fig. 1. Likewise, intrinsic broadening also will affect the line shape. Even with both limb darkening and intrinsic broadening in the model, the correlation between line width and equatorial projected rotational velocity is linear and thus measured values of line widths can be inverted to derive  $v_e$ .

Now, for rapidly rotating stars, one must also account for gravity darkening. According to von Zeipel’s law, the local flux is proportional to surface gravity. This effect thus reduces the contribution of the high-velocity equatorial regions to the overall line profile. We show this schematically in the right-hand panels of Fig. 1, where it can be seen that gravity darkening further narrows the photospheric absorption line. The three different line profile models are compared directly in the left-hand panel of Fig. 2.

Inversion of measured line widths now becomes tricky, as the relationship between the line width and the projected equatorial rotational velocity is no longer linear, as we show in the right-hand panel of Fig. 2. Indeed, beyond

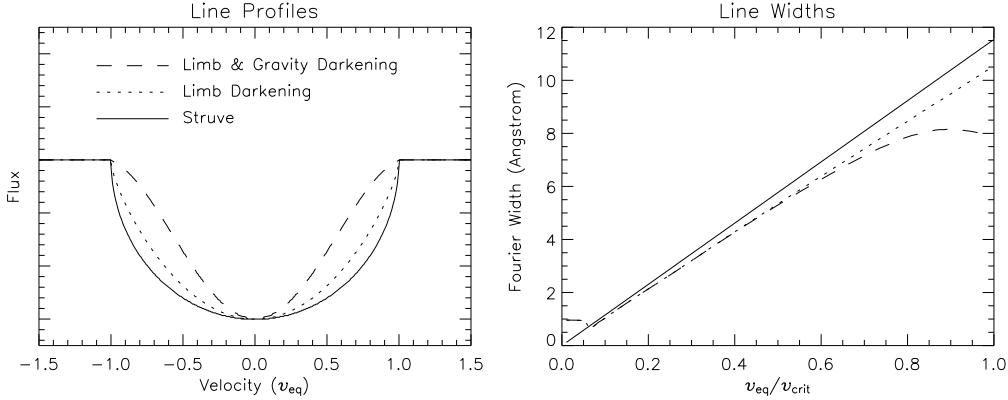


Figure 2. Left: Direct comparison of the three types of line profile – Struve, limb darkened, and gravity-darkened plus limb darkened – shown in Fig. 1. Note the progression to a narrower line as each subsequent effect is included. Right: The Fourier line width as a function of  $v_{\text{eq}}/v_{\text{crit}}$ , for the three models. The width data for the non-Struve models are based on NLTE line synthesis calculations for He I 4471 Å.

$v_{\text{eq}} \approx 0.8 v_{\text{crit}}$ , any increase in  $v_{\text{eq}}$  is accompanied by almost no change in the line width. This strong degeneracy means that classical techniques for  $v_{\text{eq}} \sin i$  determination, which neglect gravity darkening, will certainly underestimate the true projected equatorial velocity. Since a preponderance of surveys to date have used such classical approaches, it appears not unreasonable that the extant data could support an upward revision to  $v_{\text{eq}} \approx 0.95 v_{\text{crit}}$  for the majority of Be stars.

In order to address whether most Be stars are rotating this rapidly, we need multi-line diagnostics. Different lines from different ionization stages will sample different regions of a gravity-darkened star. We would expect lines with source functions weighted toward cooler temperatures to be formed preferentially near the equator while lines with source functions weighted toward hotter temperatures would be formed primarily near the poles (Townsend, Owocki, & Howarth 2004). There are other diagnostic signatures of oblateness and the associated gravity darkening, including increased UV flux that should be seen in spectra that cover far-UV wavelengths and photometric signatures of cooler equators and hotter poles. Interpreting the data, however, is difficult, as there is a need for accurate NLTE line-blanked model atmospheres in order to leverage these diagnostics. It is also possible that the observed tendency of Be stars to lie above the photometric main sequence is a hint that extreme gravity darkening must be taken into account when analyzing the spectral energy distributions of Be stars (Zorec & Briot 1991; Stoeckley 1968).

This example of the problem of inferring stellar rotational velocities from observations of photospheric absorption line widths has direct bearing on disk formation in Be stars, as many more mechanisms become viable if the material feeding the disks of these stars is already moving at  $\approx 0.95 v_{\text{crit}}$ . And it also demonstrates how even straightforward diagnostics must be tied to realistic physical models if they are to be useful. And once that is done, how we must carefully test the sensitivity of observable quantities to physically meaningful model parameters.

### 3. Polarization Diagnostics for Circumstellar Disks

Polarization diagnostics are powerful because they provide relatively direct information about the physical characteristics of circumstellar disks, even when these disks are spatially unresolved. In the case of hot stars, where dust is generally not present, the polarization is produced when starlight undergoes electron scattering in a non-spherically-symmetric circumstellar envelope (CSE). In a sense, polarization diagnostics are akin to the use of stars as “flashlights” for illuminating the interstellar medium (ISM) in absorption line studies of the ISM. Because the polarization signal arises from the scattering process, it represents a means for separation of the signature of the circumstellar material from that of the star itself. However, polarization diagnostics for hot star disks generally are not easy to interpret, as the polarization percentage is often low, and some modeling is required to interpret the observations. Solutions are not always unique, and it is always necessary to correct for the interstellar contribution (if any) to the polarization signal.

The best approach for utilizing polarization diagnostics is to combine polarization observations (preferably from different wavelengths) with other types of observational techniques, such as spectroscopy, photometry, interferometry, and imaging. Different wavelength regions probe different spatial regions, allowing for a more consistent picture of the circumstellar environment. Combination with other techniques can often provide information that will distinguish between potential non-unique solutions to polarization models. In this section we briefly discuss imaging polarimetry, spectropolarimetry, and the removal of interstellar polarization.

Although synchrotron radiation, transport through magnetically aligned grains in the ISM, and dust scattering all lead to polarization, in this work we will focus primarily on electron (Thomson) scattering, which is responsible for the polarization from hot star disks, and which is inherently wavelength independent. We also focus on linear polarization only (circular polarization diagnostics of magnetic fields are discussed elsewhere in these proceedings), using the Stokes parameter formalism (Stokes 1852; Chandrasekhar 1946); for a good discussion, see Tinbergen (1996). The observables (as a function of wavelength) are the polarization position angle and the net polarization level (in percent). The polarization level can be quite small (1-2% or less) if the polarized signal of scattered light is diluted by the unpolarized direct light from the star, as is the case for most hot star disks.

Imaging polarimetry is a useful diagnostic of YSOs with disks. Images of these objects are dominated by scattered light (e.g., Burrows et al. (1999); Wood et al. (1998), especially when the viewing angle is near the disk plane. Monte Carlo modeling of linear polarization maps can provide a tool for determining the inclination of the disk (Whitney & Wolff 2002). For detection purposes, as shown by Wisniewski et al. (these proceedings), imaging polarimetry of multiple point sources in a field, when combined with H-alpha emission selection criteria, is an effective means for identifying candidate disk systems.

Linear polarization, caused by electron scattering in CSEs, generates a polarization vector that is perpendicular to the orientation of the disk (except if the disk is very optically thick). This is shown schematically in Fig. 3. Since

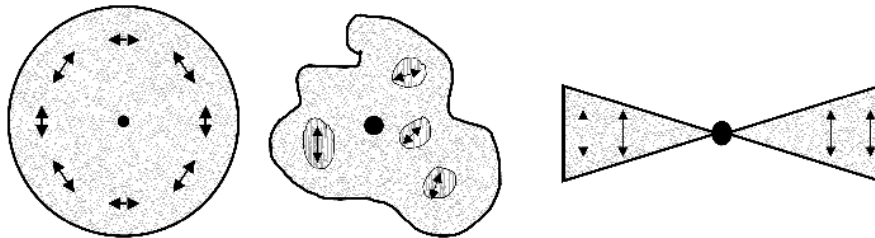


Figure 3. Schematic view of polarization production in various CSE geometries. When the CSE is unresolved, the net polarization observed will be the co-addition of all polarization produced. Left: A spherical, homogeneous distribution of scatterers will produce zero net polarization. Center: A non-spherical, non-homogeneous, “blobby” distribution of scatterers may produce a net polarization, but it will depend on the number, spatial distribution, and relative densities of the blobs. If the blobs are time-variable, the observed polarization will also be variable. Right: A disk-like distribution of scatterers will produce a net polarization with a position angle perpendicular to the disk, because there is little or no cancellation due to polar material.

the CSEs are not spatially resolved, the observed signal is the coadded net polarization. As a result, the polarization position angle gives a measurement of the orientation of the disk on the sky, even when the disk is not resolved.

While the electron scattering polarization is wavelength independent, the observed polarization does show a wavelength dependence. This happens because of the pre- and post-scattering attenuation of polarized light by the disk material as the photons work their way through the disk (Wood & Bjorkman 1995; Wood et al. 1996a,b). When the absorption cross sections are larger, less polarized flux will escape from the disk, and so the net polarization measured will be smaller at those wavelengths. This effect means that the polarization “spectrum” can provide a direct probe of the physical conditions of the disk material, including temperature and density.

Thus, the measured intrinsic polarization depends on the disk geometry, density, and temperature (which affects the opacity). As an example, we show an observation of  $\zeta$  Tau in Fig. 4, along with Monte Carlo model calculations of the percent polarization versus disk opening angle. As this figure shows, there is a degeneracy in the opening angle determination. However, when combined with  $H\alpha$  interferometry (Quirrenbach et al. 1997), the large opening angle can be ruled out, and the small opening angle value is determined to be the correct one.

The results from the types of studies described above show that Be star disks are surprisingly thin, with typical opening angles of only 2.5 degrees. These opening angles are consistent with disk thicknesses that would be predicted by models of pressure-supported (Keplerian) disks, although the polarization observations do not themselves provide direct evidence that the disks

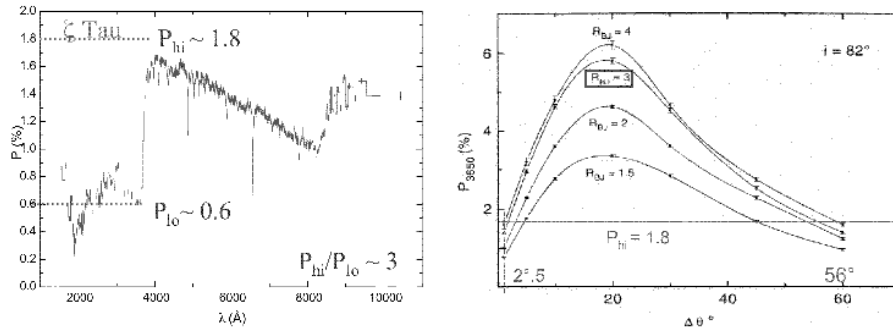


Figure 4. Left: Spectropolarimetric data from the UV through the optical for the Be star  $\zeta$  Tau. Right: Monte Carlo calculations of the peak polarization level as a function of disk opening angle for several values of the Balmer jump polarization ratio. Figures adapted from Wood, Bjorkman, & Bjorkman (1997). The inclination angle of the disk was assumed to be 82 degrees (nearly edge-on), consistent with the location of  $\zeta$  Tau in the “triangle diagram” of Coté & Waters (1987).

are Keplerian. Studies of the opacity of the disk material from spectropolarimetry allow a determination of temperature and disk densities. Derived disk temperatures for the inner region of the circumstellar disk (where most of the polarization is produced) are typically 75% of the stellar effective temperature (Bjorkman, Bjorkman, & Wood 2000). These results show how multi-wavelength, multi-technique observations and diagnostics supported by modeling can provide quantitative, physical information about circumstellar environments.

It is also important to note that models developed for the purpose of explaining other observed phenomena generally will also carry implications for expected polarization, whether the models were intended for this purpose or not! Polarization observations thus can be used as an additional test for the validity of such models. An example of this is shown by (McDavid et al. 2000), looking at V/R variations in H $\alpha$  line profiles of Be stars and their interpretation in the context of models of one-armed spiral density waves. They conclude that while the models do a reasonable job of reproducing the general character of the spectral variations, the density waves would also produce specific temporal variations in the polarization level. The existing polarimetric data at the time of this study did not have sufficient time coverage or sensitivity to detect whether these polarization variations were observed or not.

Finally, we note that to study intrinsic polarization and fully utilize its diagnostic power, interstellar effects need to be removed. This is often quite difficult due to spatial variation in interstellar polarization (ISP), distance uncertainties, and a lack of complete catalogs of polarization measurements for large numbers of stars all across the sky. One technique that can be applied to Be stars, where

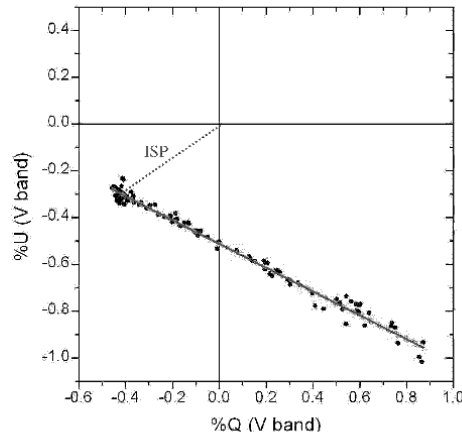


Figure 5. A Stokes QU plot showing the time variability of the V-band equivalent polarization of the Be star  $\pi$  Aqr. When the intrinsic polarization is at its lowest state, with the disk dissipated (or nearly so), the polarization level is only due to the contribution of the interstellar polarization (ISP). At this point, the ISP vector can be determined, as indicated by the dashed line (labeled ISP) running from (0,0) to the ISP value.

disks form and dissipate and then reform on relatively short timescales, is to monitor the polarization over time. In the Q-U plane, each observation represents a point, and the interstellar contribution can be represented as a vector that shifts each point from its intrinsic value. During monitoring, if observations are made at a time when the disk has dissipated (determined based on H $\alpha$  or IR diagnostics) then the interstellar polarization vector can be determined and (retroactively) applied to all the other points in the Q-U plane (see Fig. 5). Further information about methods for removing the ISP is discussed in some detail in Quirrenbach et al. (1997).

Some of the prospects for the future of polarimetric diagnostics include SPIN (SpectroPolarimetric INterferometry; cf. Chesneau, et al. (2003)); polarimetric differential imaging (e.g., Apai et al. (2004)); Integral Field Unit (IFU) spectropolarimetry, which allows for spectropolarimetry of many sources in one field simultaneously; and new polarimetric capabilities on larger telescopes. This last item will allow for detailed polarimetry of fainter sources and higher resolution spectropolarimetry. For an excellent overview of the wide range of modern polarimetric instruments, techniques, and astronomical applications, as well as previews of developing capabilities, the reader is referred to the many papers contained in the proceedings of the recent conference on Astronomical Polarimetry (Adamson et al. 2004).



#### 4. X-ray Line Diagnostics of the Magnetic O Star $\theta^1$ Ori C

$\theta^1$  Ori C (O7 V), the ionizing source of the Orion Nebula, exhibits periodic H $\alpha$  emission, variable FUV P-Cygni profiles, and X-ray emission (Stahl et al. 1996; Gagné et al. 1997). Its dipole magnetic field strength shows the same 15.4-day periodicity, with the magnetic pole in the line of sight at X-ray and H $\alpha$  emission maximum (Donati et al. 2002). These multiwavelength variability properties have long been interpreted in terms of an oblique magnetic rotator model.

Interestingly, it wasn't until the optical spectroscopic magnetic field measurements that the H $\alpha$  and UV observations could be correctly interpreted, and a coherent unified picture of the magnetically controlled circumstellar envelope of this hot star was established. Strong, hard, variable X-ray emission was predicted by Babel & Montmerle (1997), assuming wind material was confined within a rigid magnetosphere, leading to shocks and a cooling disk at the magnetic equator. In the Babel & Montmerle interpretation, the X-rays were *weaker* when the star is viewed pole-on because of absorption in the dense cooling disk. The later magnetic field measurements of Donati et al. (2002) directly contradicted that prediction. It turns out that the longitudinal magnetic field is weakest at  $\phi = 0.5$ , when the X-ray and H $\alpha$  emission are also at their lowest levels but the UV absorption excess is maximized. The coherent picture that emerges is thus one where the circumstellar material at the magnetic equator is associated with X-ray and H $\alpha$  emission that is occulted at  $\phi = 0.5$  by the star, and the wind flow along the magnetic equator thus maximizes the UV absorption at the same phase.

The MHD model of ud-Doula & Owocki (2002) was applied to this problem (see Oksala et al. in these proceedings), showing that the radiatively driven wind distorts the magnetic geometry, creating an outflowing disk at large radii and strong, relatively high-density shocks above and below the magnetic equator from  $R = 1.2 - 2R_*$ . The high-resolution spectroscopy available with the *Chandra* gratings provides several useful diagnostics for analyzing the spatial extent, temperature, and kinematics of the magnetically confined, shocked plasma in the circumstellar environment of this star. The geometry of the magnetosphere, as determined from the multiwavelength optical and UV observations described above is summarized in Fig. 6 which also shows the viewing angle for four separate *Chandra* pointings.

The most common type of X-ray spectral diagnostic applied to *Chandra* grating spectra of stars is the fitting of optically thin thermal emission models (e.g., APEC) to the entire spectrum to determine the column density of absorbing material overlying the X-ray emitter and the temperature(s), abundances, and volume emission measure of the X-ray emitting plasma. This emission measure analysis shows very hot plasma ( $T \approx 30$  MK), approximately solar abundances for most elements and substantially sub-solar Fe. The emission measure decreases by  $\approx 35\%$  from maximum to minimum, but the other parameters do not vary significantly, suggesting that the X-ray emitting region is close to the star ( $R < 1.5R_*$ ) and is occulted by the star as the star and the closed magnetic regions rotate once every 15.4 days.

X-ray emission line widths provide information about plasma kinematics. Unlike the standard instability-driven wind shock sources among the O stars,

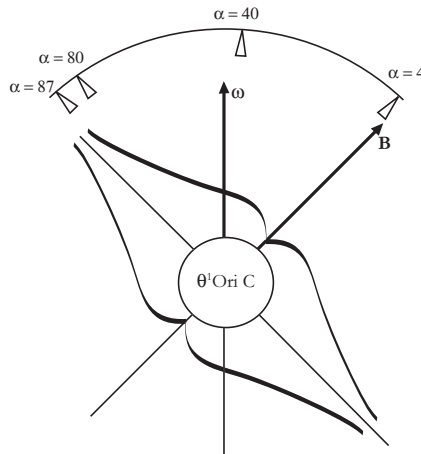


Figure 6. Schematic of  $\theta^1$  Ori C and its circumstellar environment, with a magnetic obliquity of  $\beta = 42^\circ$ . The viewing angles with respect to the magnetic pole are indicated by the four labels at the top of the diagram. In this view, the observer does not change position from observation to observation, but rather the star and its magnetic field rotate, providing a fixed observer different perspectives. X-ray maximum occurs near viewing angle  $\alpha = 3^\circ$ .

which have broad and asymmetric profiles,  $\theta^1$  Ori C has narrow, though well-resolved, X-ray emission lines. As we show in Fig. 7, the characteristic velocity of the emission lines is only  $300 \text{ km s}^{-1}$ , compared with  $v_\infty = 2000 \text{ km s}^{-1}$  seen in the stellar wind. The very hot plasma is moving, but at speeds much less than the ambient wind speed. Interestingly, a few of the X-ray emission lines, from the coolest plasma component, show larger widths, consistent with instability-driven wind shocks. But the harder X-rays from hotter plasma shows behavior consistent with some degree of magnetic confinement.

Aside from the line-profile analysis, spectral fitting, and time-variability analysis, high-resolution X-ray spectra can provide one other plasma diagnostic. The ratio of forbidden-to-intercombination ( $f/i$ ) line strength in helium-like ions can be used to measure the electron density of the X-ray emitting plasma and/or its distance from a source of FUV radiation, like the photosphere of a hot star (Blumenthal, Drake, & Tucker 1972). The left panel of Fig. 8 is an energy-level diagram for S XV similar to the one for O VII first suggested by Gabriel & Jordan (1969). It shows the level energies (eV) and transition wavelengths ( $\text{\AA}$ ) of the resonance ( $^1P_1 \rightarrow ^1S_0$ ), intercombination ( $^3P_{2,1} \rightarrow ^1S_0$ ), and forbidden ( $^3S_1 \rightarrow ^1S_0$ ) lines. Aside from the usual collisional excitations (solid lines) and radiative decays (dashed lines), the metastable  $^3S_1$  state can be depopulated by collisional and/or photo-excitation to the  $^3P$  states. In late-type stars, the  $f/i$  ratios of low-Z ions like N VI and O VII are sensitive to changes in electron density near or above certain critical densities (typically in the  $10^{12} \text{ cm}^{-3}$  regime). Higher-Z ions have higher critical electron densities typically not seen in normal (non-degenerate) stars. Kahn et al. (2001) have used the  $f/i$  ratios of N VI, O VII, and Ne IX and the radial dependence of the incident UV flux to determine that most of the emergent X-rays from the O4

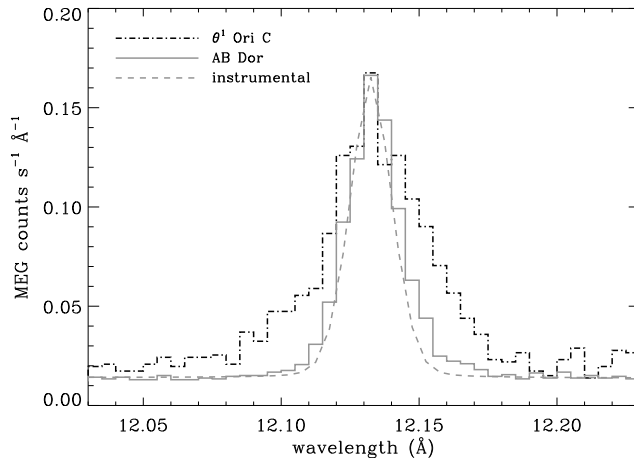


Figure 7. The neon Lyman alpha line in the *Chandra* MEG spectrum of  $\theta^1$  Ori C compared to the same line seen in the MEG spectrum of the active young M dwarf, AB Doradus. An absolutely narrow model convolved with the MEG instrumental response is also shown for comparison. The  $\theta^1$  Ori C line is clearly broad.

supergiant  $\zeta$  Pup were formed in the far wind, consistent with radiatively-driven wind shocks.

In  $\theta^1$  Ori C, the low-Z forbidden lines are completely suppressed. The right-hand panel of Fig. 8 shows the resonance, intercombination, and forbidden lines of Mg XI and Ar XVII. Modeling the excitation kinematics of these lines at the dominant plasma temperature of 33 MK, the undetected Mg XI forbidden line suggests a formation radius  $R < 1.8R_*$  while the S XV  $f/i$  ratio provides  $1\sigma$  lower and upper bounds of 1.2 and  $1.5R_*$ , consistent with Mg XI. The Si XIII lines have the highest S/N, but the forbidden line is blended with a strong line of Mg XII. That said, the Si XIII lines and the lower-S/N Ar XVII lines are consistent with the S XV measurement, i.e., less than approximately half a stellar radius above the photosphere. This is also consistent with the reduction in emission measure seen near phase 0.5, based on the geometry of the occultation and the depth of the dip in the X-ray light curve.

All of these X-ray diagnostics, and the earlier optical and UV observations, can be understood in terms of a model in which a radiation-driven wind is channeled by a dipole magnetic field toward the magnetic equator where flows from the two hemispheres collide and shock-heat. This picture has been confirmed by numerical MHD simulations. These simulations, based on those of ud-Doula & Owocki (2002), show that the magnetically channeled flows are confined within about a stellar radius of the photosphere, i.e.,  $R \approx 1 - 2R_*$ , where they shock heat plasma to approximately 30 MK, producing relatively narrow, symmetric, X-ray emission lines.

This analysis demonstrates the power of quantitative X-ray spectral diagnostics to determine the values of physically meaningful parameters related to circumstellar matter in magnetic hot stars. This situation is only possible, however, because of the existence of quality datasets in the optical and UV to

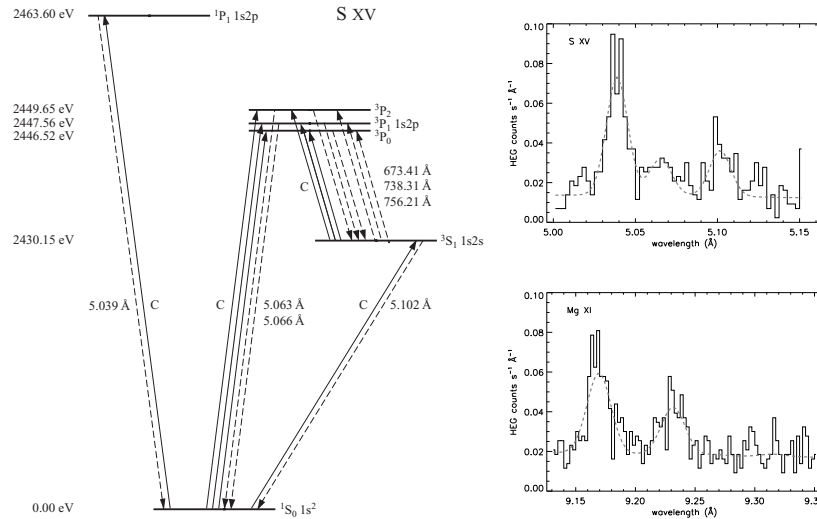


Figure 8. Energy-level diagram for S XV (left) after Gabriel & Jordan (1969). Collisional excitations (C) are shown with solid lines; radiative decays are shown with downward pointing dashed lines; photo-excitation is shown with upward pointing dashed lines. APED level energies and observed transition wavelengths are also noted. Electrons are excited out of the  $3S_1$  level (by collisions at high density and by radiation close to a hot photosphere), leading to suppression of the forbidden line (labeled by its wavelength, 5.102 Å), and enhancing the intercombination line (5.063, 5.066 Å). The two panels on the right show the observed He-like S and Mg *fir* complexes along with best-fit models. The forbidden line, which is the component at the long-wavelength end of each spectral region, is moderately strong in the sulfur but is suppressed by photoexcitation in the magnesium.

augment the X-ray data, and, importantly, because of the numerical models of the magnetic wind of  $\theta^1$  Ori C that makes quantitative predictions that the data can be used to test.

Finally, we note that the circumstellar envelope of this star is not a true disk, in the sense of Be stars, for example, where the circumstellar envelope is thin and orbitally supported. In  $\theta^1$  Ori C, the envelope is more toroidal and is supported, but only temporarily, by the magnetic field. Prospects for finding other stars in this category - young hot stars with magnetically controlled circumstellar matter - involve identifying hard and variable X-ray sources, and then combining those data with H $\alpha$  emission and UV absorption measurements. So far, about a dozen such O-, B-, and A-type candidates, mostly spectroscopic binaries, have been identified in the Orion Nebula region.

## 5. Conclusions

The field of diagnostics is an extraordinarily broad and diverse one, and in this paper we have touched on only three rather specific diagnostics and their associated applications. However, while there is both a certain amount of common ground as well as some interesting differences among these three examples, sev-

eral underlying lessons emerge. First of all, researchers must be aware of their biases and always be leery of the assumptions that underly the models that they rely on to interpret data. Employing models to interpret data is of crucial importance, though, as determining physical parameters of interest is the ultimate motivation for employing diagnostics in the first place.

The section on absorption line profiles and Be star rotational velocities shows that even traditional diagnostics must be tied to models in order to provide meaningful physical interpretations, and that the assumptions behind models should be reevaluated periodically as theories become more sophisticated. Also, observers must not lose sight of which specific properties of the observational data are sensitive to the physical parameters of interest. The section on polarization diagnostics demonstrates how the electromagnetic radiation we measure contains a huge amount of information that can be extracted if the diagnostics are interpreted in light of physical models. And, like so many diagnostic techniques, there are flies in the ointment (in this case, the removal of interstellar polarization) that can be difficult to deal with, but which must be accounted for if meaningful conclusions are going to be drawn from the data. This case is especially satisfying because it is in fact one of the inherently interesting properties of the class of objects under study – namely the rapid dispersal and then formation of Be disks – that enables us to make an accurate assessment of ISP contamination. Finally, the section on  $\theta^1$  Ori C presents a nearly unique case that nonetheless illustrates some of the basic guidelines for employing observational diagnostics. In this final section, we see again how important it is to have an underlying physical model for the interpretation of diagnostics. We also see how combining data at several wavelengths is vital. And finally we see how important quantitative measurements of specific physical properties (e.g. X-ray line widths and line ratios) are for making meaningful progress in understanding astrophysical systems of interest.

## References

- Adamson, A., Aspin, C., Davis, C., & Fujiyoshi, T. (editors) 2004, “Astronomical Polarimetry: Current Status and Future Directions”, ASP Conf. Proc., in press.
- Apai, D., Pascucci, I., Brandner, W., Henning, T., Lenzen, R., Potter, D. E., Lagrange, A.-M., & Rousset, G. 2004, *A&A*, 415, 671
- Babel, J., & Montmerle, T. 1997, *ApJ*, 485, L29
- Bjorkman, K. S., Bjorkman, J. E., & Wood, K. 2000, IAU Colloq. 175: The Be Phenomenon in Early-Type Stars, (ed. M. Smith and H. Henrichs), ASP Conf. Ser., 214, 603
- Blumenthal, G. R., Drake, G. W. F., & Tucker, W. H. 1972, *ApJ*, 172, 205
- Burrows, S. 1999, *ApJ*, 516, L95
- Chandrasekhar, S. 1946, *ApJ*, 104, 110
- Chesneau, O., Wolf, S., & Domiciano de Souza, A. 2003, *A&A*, 410, 375
- Coté, J., & Waters, L.B.F.M. 1987, *A&A*, 176, 93
- Donati, J.-F., Babel, J., Harries, T. J., Howarth, I. D., Petit, P., & Semel, M. 2002, *MNRAS*, 333, 55
- Gabriel, A. H. & Jordan, C. 1969, *MNRAS*, 145, 241
- Gagne, M., Caillault, J., Stauffer, J. R., & Linsky, J. L. 1997, *ApJ*, 478, L87
- Kahn, S. M., Leutenegger, M. A., Cottam, J., Rauw, G., Vreux, J.-M., den Boggende, A. J. F., Mewe, R., & Güdel, M. 2001, *A&A*, 365, L312

- McDavid, D.A., Bjorkman, K.S., Bjorkman, J.E., & Okazaki, A.T. 2000, in IAU Colloq. 175: The Be Phenomenon in Early-Type Stars, (ed. M. Smith and H. Henrichs), ASP Conf. Ser., 214, 460
- Quirrenbach, A., et al. 1997, ApJ, 479, 477
- Tinbergen, J. 1996, *Astronomical Polarimetry*, (Cambridge: Cambridge Univ. Press), Ch. 2
- Townsend, R. H. D., Owocki, S. P., & Howarth, I. D. 2004, MNRAS, 350, 189
- Shajn, G., & Struve, O. 1929, MNRAS, 89, 222
- Stahl, O. et al. 1996, A&A, 312, 539
- Stoeckley, T. R. 1968, MNRAS, 140, 141
- Stokes, G. G. 1852, *Trans. Camb. Phil. Soc.*, vol. 9, pt. III, pp. 399-416.
- ud-Doula, A. & Owocki, S. P. 2002, ApJ, 576, 413
- Whitney, B.A. & Wolff, M.J, 2002, ApJ, 574, 205
- Wood, K., & Bjorkman, J.E. 1995, ApJ, 443, 348
- Wood, K., Bjorkman, J.E., Whitney, B.A., & Code, A.D. 1996, ApJ, 461, 828
- Wood, K., Bjorkman, J.E., Whitney, B.A., & Code, A.D. 1996, ApJ, 461, 847
- Wood, K., Bjorkman, K.S., & Bjorkman, J.E. 1997, ApJ, 477, 926
- Wood, K., Kenyon, S.J., Whitney, B., & Turnbull, M. 1998, ApJ, 497, 404
- Zorec, J. & Briot, D. 1991, A&A, 245, 150